IIUC Journal of Science and Engineering
Vol.-2, Issue-1, December 2024, pp. 09-28
ISSN: 3005-5873

Photovoltaic efficacy of WS_2 as back surface field (BSF) and SWCNT as an absorber layer for heterostructure solar cell: Numerical investigation by SCAPS-1D multidimensional framework

Muhammad Athar Uddin
Department of Electrical and Electronic Engineering
International Islamic University Chittagong (IIUC), Bangladesh

Article info

Keywords
Single-walled carbon nanotube
Composite solar cell structure
Back Surface Field
SCAPS-1D

Abstract

This study presents a highly efficient heterostructure solar cell model using single-walled carbon nanotubes (SWCNTs) as the absorber layer, tungsten di-sulfide (WS_2) as BSF layer and platinum (Pt) as the back contact. Using the SCAPS-1D software, the research focuses on optimizing critical design parameters such as the thickness (W) and acceptor concentration (N_A) of the absorber layer, along with the impact of as the BSF series-shunt resistance, temperature and defect densities across different layers. The model, ITO/CdS/SWCNT/WS_2 configurations, aims to achieve superior PV performances. Key innovations include the incorporation of minority carriers to simulate defects and interfaces defect coefficients depicted through contour plots. The optimized parameters for the ITO/CdS/SWCNT/WS_2 model are established at a thickness of 1.5 μm, an acceptor concentration of $4\times10^{19}cm^{-3}$ and a defect density of $1\times10^{16}cm^{-3}$, resulting in an efficiency of 30.01% with V_{OC} = 0.86V, J_{SC} = 41.42mA/cm^2 and FF = 83.84% achieved at 300^{o}K temperature. These discoveries underscore the considerable promise of SWCNTs functioning as the absorber layer in a heterostructure solar cell, offering promising outcomes for environmental sustainability and global energy solutions

Corresponding author
Muhammad Athar Uddin
Department of Electrical and Electronic Engineering, International Islamic University Chittagong, Kumira, Chattogram, Bangladesh - 4318
Email: mau_iiuc@yahoo.com

1. Introduction

The quest for high-efficiency solar cells is a pivotal aspect of advancing renewable energy technologies, addressing the escalating demand for sustainable energy sources (Parida, Iniyan, & Goic, 2011; Ray &

Chakraborty, 2021; Scheer, 2004). In the past few years, the development of heterostructure PV cells has received notable interest because of their potential to surpass the efficiency limits of traditional photovoltaic cells (Andreev, 1999; Idisi & Mwakikunga, 2023; Niu et al., 2022; Wang, Liu, Konik, Misewich, & Wong, 2013). This study delves into the innovative design of a heterostructure solar cell model, leveraging the distinct characteristics of single-walled carbon nanotubes (SWCNTs) as the absorber layer (Gorji & Houshmand, 2013; Hata et al., 2004; Daniel D. Tune et al., 2013), tungsten disulfide (WS_2) as the BSF layer, and platinum (Pt) as the back contact. The incorporation of SWCNTs as the absorber layer is particularly noteworthy, given their exceptional electronic properties (Bati et al., 2019), including high electron mobility and tunable band gaps (Aitola et al. 2016; Barbero and Stranks 2016), which are conducive to enhanced photovoltaic performance. The use of WS_2 as the BSF layer introduces further advantages as it can be used as a p-type layer in the solar cell (Khatun, Sunny, & Ahmed, 2021), such as improved charge separation and reduced recombination losses, contributing to the entire performance of the photovoltaic cell. Regrettably, the photovoltaic performance of traditional WS_2-based solar cells rarely matches the effectiveness of commercially available thin-film solar cells (TFSCs). This limitation is likely due to Fermi level pinning limits the attainment of a high V_{OC} (Nazif, Kumar, Menezes, & Saraswat, 2019). Therefore, this work opens up with this opportunity to use tungsten di-sulfide as BSF with a single-walled carbon nanotube (SWCNT) absorber as it shows higher efficiency by using it at the absorber in the previous studies (Subash & Chowdhury, 2009).

Single-walled carbon nanotubes with semiconducting properties (s-SWCNTs) are considered excellent prospects for the photo-absorptive component in cost-efficient, flexible solar panels due to their effective absorption in the near-infrared (NIR) spectrum and superior electron mobility (Arnold et al., 2013; Dürkop, Getty, Cobas, & Fuhrer, 2004; Schöppler et al., 2011). Adjusting the diameter of these nanotubes enables the fine-tuning of their bandgaps, facilitating precise alignment with specific segments of the solar spectrum (Bachilo et al., 2002). For example, sophisticated simulations involving solar cells composed of four varied diameters of SWCNTs indicate an anticipated efficiency in solar energy conversion between 19% and 28%. This range depends on the size of the bandgap, with larger bandgaps capturing up to 28% efficiency predominantly in the visible spectrum, and smaller ones achieving 19% in the NIR spectrum (Daniel David Tune & Shapter, 2013). This customizable optical characteristic is especially valuable for emerging

technologies like photovoltaic windows integrated into buildings, which demand both significant NIR absorption and substantial transparency in the visible spectrum. This research aims to address the challenges related to solar cell efficiency by optimizing the specified parameters to attain improved performance metrics, such as V_{OC} (V), J_{SC} (mA/cm^2), FF (%) and η (%). Previously a few researchers Xosrovashvili and Gorji, (2014), Uddin, Rafi, Islam, Mominuzzaman, and Nath, (2022), Islam, Al Rafi, and Uddin, (2023), Oublal, Ait Abdelkadir, and Sahal, (2022) introduced SWCNT based heterostructure solar cell with a remarkable outcome. But in those studies investigation for solar cell by numerically were limited and the defects level were maintained below from this study. The design parameters, including the absorber layer's thickness and acceptor concentration, alongside series-shunt resistance, temperature effects, and defect densities, are meticulously optimized using the SCAPS-1D software.

In this study, the optimized ITO/CdS/SWCNT/WS_2 solar cell model demonstrates a remarkable efficiency of 30.01%, with V_{OC} = 0.86V, J_{SC} = 41.42mA/cm^2, and FF = 83.84% at an operational temperature of 300K, thickness of 1.5 μm, an acceptor concentration of 4×10^{19}cm^{-3}, and a defect density of 1×10^{16}cm^{-3}. These findings underscore the significant likelihood of SWCNTs in heterostructure solar cells, facilitating the way for future research and development in nanostructured photovoltaic materials. The promising outcomes of this study highlight the role of advanced material engineering in achieving environmental sustainability and addressing global energy challenges through innovative solar cell technologies. This research utilizes tungsten disulfide (WS_2) as a BSF layer, which is notable for improving charge separation and reducing recombination losses. The potential use of WS_2 as a p-type layer in solar cells opens new avenues for enhancing the effectiveness of hybrid cells. The detailed simulation using SCAPS-1D software to optimize critical design parameters like thickness, acceptor concentration, series-shunt resistance, temperature effects, and defect densities represents a comprehensive approach to maximizing solar cell efficiency. The literature and comparative studies have been discussed with similar previous works for better understanding of the improvement in this relevant field. In a physical experiment, the structure with the same parameters might show a less outcome than simulation for the actual defects and the materials with their individual minorities. As for this structure individual defects and interface defects were tried to keep higher than previous studies, still it's showing the better outcomes. The focus on minority carriers to simulate defects and interfaces, along with the detailed contour plots provided, adds depth to the understanding of material behavior under operational

conditions. This aspect of this research enhances the physical realism and predictive accuracy of your simulations.

2. Computational device modeling and simulation specifications

The structure proposed in this study, Al/ITO/CdS/SWCNT/WS_2/Pt, was evaluated using numerical simulations conducted with the SCAPS-1D (a Solar Cell Capacitance Simulator) simulator. SCAPS-1D is a one-dimensional simulator based on the steady-state solution of three fundamental equations governing semiconductor devices: Poisson's equation and the equations governing the flow of free holes and electrons. (Burgelman, Nollet, & Degrave, 2000). Poisson's equation considers charge distribution and electric field, showing the solar cell's electrostatic potential, whereas the continuity equation links the processes of carrier creation, recombination, and transport.

The Poisson equation is given by:

$$div(\varepsilon\nabla\Psi) = -\rho \quad (1)$$

The continuity equation for free electrons is expressed as:

$$\frac{\partial n}{\partial t} = \frac{1}{q} div\vec{j}_n + G_n - R_n \quad (2)$$

The continuity equation for free holes is defined as:

$$\frac{\partial p}{\partial t} = \frac{1}{q} div\vec{j}_p + G_p - R_p \quad (3)$$

This computer-based simulator operates by inputting the electrical and optical parameters for each defined layer. It enables the modeling of physical and electronic structures of heterojunctions, homojunctions, multi-junctions, and Schottky barriers. The simulator allows for the adjustment of individual input parameters for each layer. The final planar device structure of the solar cell is illustrated in Fig. 1. This substrate-type structure is chosen due to its technological feasibility and proven success in SWCNT-based solar cells.

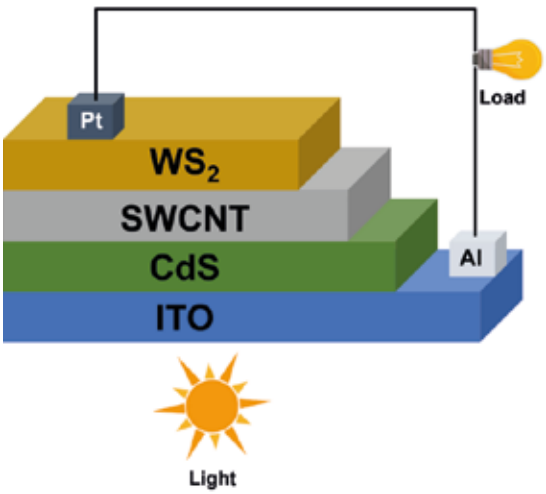

Figure. 1
Device Structural model of the proposed model (Al/ITO/CdS/SWCNT/WS_2/Pt).

Table. I
Parameters Utilized for Simulating the ITO/CdS/SWCNT/WS_2 Heterostructure Cell (Khatun et al., 2021; Oublal et al., 2022; Rahman, 2021; Xosrovashvili & Gorji, 2014)

Parameters	ITO	CdS	SWCNT	WS_2
Thickness (μm)	0.05	0.05	0.5 – 3.0	1.0
Bandgap E_g (eV)	3.6	2.4	1.10	1.29
Electron Affinity, χ (eV)	4.5	4.3	4.27	4.05
Dielectric Permittivity	8.9	8.73	3.40	13.6
CB effective density of states (cm^{-3})	2.2×10^{18}	2.2×10^{18}	5.0×10^{16}	2.2×10^{18}
VB effective density of states (cm^{-3})	1.8×10^{19}	1.8×10^{19}	6.0×10^{17}	1.8×10^{19}
Electron Thermal Velocity (cms^{-1})	1.0×10^{7}	1.0×10^{7}	1.0×10^{7}	1.0×10^{7}
Hole Thermal Velocity (cms^{-1})	1.0×10^{7}	1.0×10^{7}	1.0×10^{7}	1.0×10^{7}
Electron mobility, μ_n ($cm^2V^{-1}s^{-1}$)	50	160	8.0×10^{4}	100
Hole mobility, μ_p ($cm^2V^{-1}s^{-1}$)	10	15	2.0×10^{3}	100
Donor concentration, N_D (cm^{-3})	1.0×10^{16}	1.0×10^{17}	0.0	0.0
Acceptor concentration, N_A (cm^{-3})	0.0	0.0	4.0×10^{15} – 4.0×10^{20}	1.0×10^{17}

The key input parameters for the simulation representing physical aspects are detailed in Table I. The donor concentration (N_D) in the first layer (ITO) is kept lower (less than 1×10^{17} cm^{-3}) to facilitate thermionic emission (TE). When N_D exceeds 1×10^{19}, tunneling occurs within the layer, leading to ohmic contact (Schroder & Meier, 1984). The thickness and acceptor concentration of the absorber layer (SWCNT) have been

adjusted between 0.5 to 3.0 μm and 4.0×10^{15} cm^{-3} to 4.0×10^{20} cm^{-3}, respectively, to determine optimal results.

Table. II
Font and Back contact parameters.

Parameters	Back contact electrical properties	Font contact electrical properties
	Pt	Al
Surface recombination velocity of electrons (cms^{-1})	1.00E+5	1.00E+7
Surface recombination velocity of holes (cms^{-1})	1.00E+7	1.00E+5
Work Function (eV)	5.65	4.26

Table II delineates the parameters governing the front and back contacts utilized in this research. Notably, the surface recombination velocity parameter is inversely applied for electrons and holes, a concept elucidated in prior published research (Atowar Rahman, 2021). Moreover, specific work functions are assigned to each contact.

2.1 Defects analysis

Table. III
Parameters pertaining to defects at three interfaces.

Parameters	ITO/CdS	CdS/SWCNT	SWCNT/WS_2
Defect type	Neutral	Neutral	Neutral
Capture cross-section of electrons (cm^2)	1.0×10^{-19}	1.0×10^{-19}	1.0×10^{-19}
Capture cross-section of holes (cm^2)	1.0×10^{-19}	1.0×10^{-19}	1.0×10^{-19}
Energetic distribution	Single	Gaussian	Single
Total defect density(cm^{-2})	1.0×10^{16}	1.0×10^{16}	1.0×10^{16}

To physically model a heterostructure cell, a composite comprising suitable semiconductors is essential. Semiconductors typically require minority and crystal defects to establish a junction. Table III displays the interface defect parameters for three interfaces formed with: i. n-type/n-type, ii. n-type/p-type, and iii. p-type/p-type.

Table. IV
Defect parameters of individual layers

Parameters	At each layer (ITO, CdS, SWCNT & WS_2)
Defect type	**Neutral**
Capture cross section electrons (cm^2)	**1.0×10^{-15}**
Capture cross section holes (cm^2)	**1.0×10^{-15}**
Energetic distribution	**Single**
Reference for defect energy level Et	**Above EV (SCAPS < 2.7)**
Total density (cm^{-3}): uniform	**1.0×10^{16}**

Meanwhile, Table IV presents the defect parameters for individual semiconductor layers, representing a combined function of minority and crystal defects. The range of defects varies from 1.0×10^{14} to

1.0×10^{17} cm^{-3} to ensure a comprehensive evaluation and draw more reliable conclusions.

3. Simulated results and discussion

3.1 Band diagram analysis

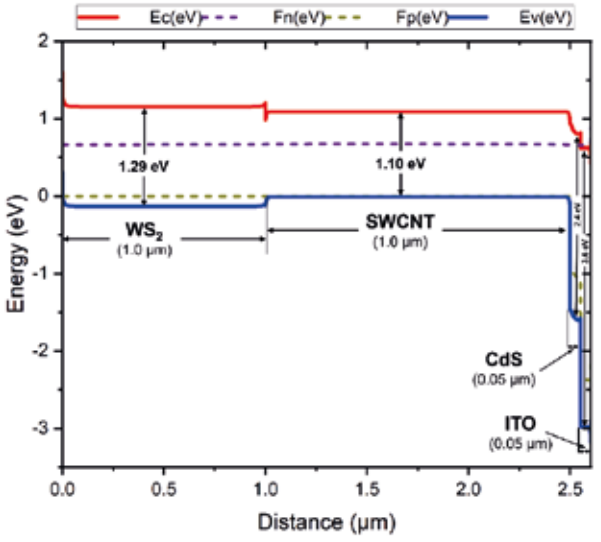

Figure. 2
Energy band diagram of the heterostructure cell comprising ITO/CdS/SWCNT/WS_2.

A band diagram, a graphical representation that illustrates various electron energy levels influenced by the PV thickness, facilitates understanding of device characteristics. Fig. 2 presents the energy band diagram of the proposed heterostructure model, with particular emphasis on the SWCNT absorber layer, which is the primary focus of this study. The band diagram depicted in this figure is optimized based on the conditions established in this research.

3.2 Combined effects of absorber layers acceptor concentration and thickness on PV outputs

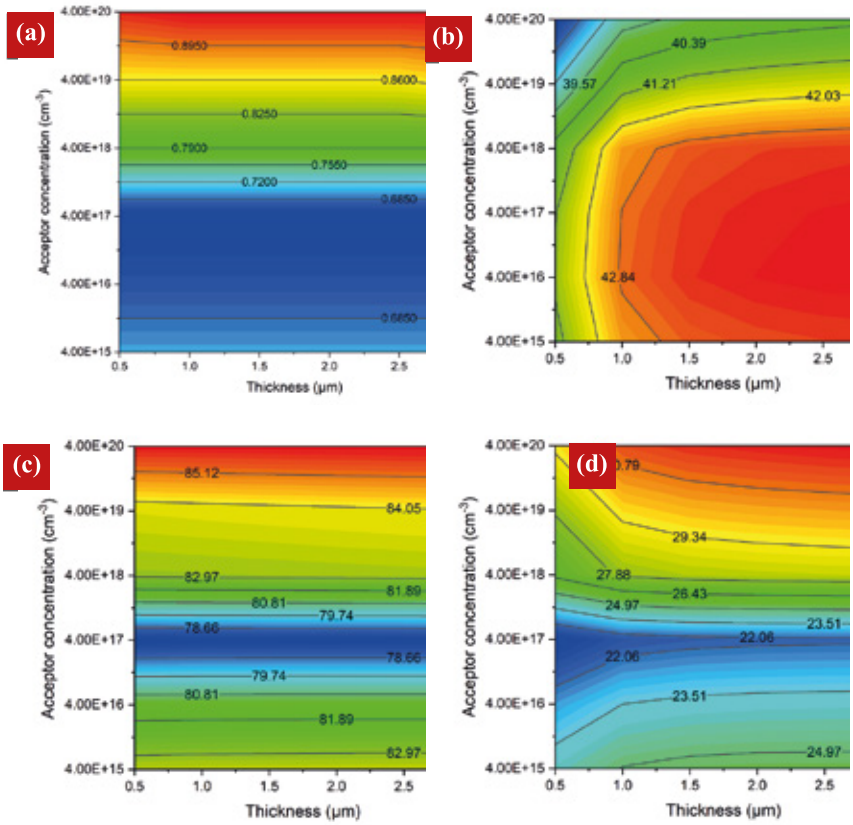

Figure. 3
Combined effects of absorber layers acceptor concentration and thickness on the performance of swcnt-based solar cells: (a) VOC, (b) JSC, (c) FF, and (d) Efficiency (%)

The primary design factors influencing solar cell performance are the acceptor concentration and the thickness of the absorber layer. To achieve optimal solar cell efficiency, it is crucial to adjust these parameters appropriately. In this study, the acceptor concentration (NA) for SWCNTs was varied from 4×1015cm-3 to 4×1020cm-3 and the thickness was adjusted from 0.5µm to 3.0µm. Fig. 3 illustrates the combined effects of acceptor concentration and absorber layer thickness on the

photovoltaic parameters VOC, JSC, FF, and efficiency (%η) for the Al/ITO/CdS/SWCNT/WS2/Pt structure. The results indicate that the absorber layer's concentration significantly influences cell performance and that the efficiency (%η) can be modified by altering the acceptor concentration in the SWCNT absorber layer. Figures 3(a) to 3(d) display the effects on open circuit voltage, short circuit current, fill factor, and overall efficiency respectively. In Fig. 3(a), the open circuit voltage (VOC) remains relatively stable with changes in the acceptor concentration but varies with the absorber layer's thickness. Higher VOC values are observed while the NA exceeds 4×1018 cm−3. Notably, increasing the carrier density in the SWCNT layer from 4×1017 to 4×1020cm−3 results in a significant rise in VOC, which can be attributed to the reduction in reverse saturation current with increased carrier concentrations. In Fig. 3(b), JSC falling down with increase of acceptor concentration but rises with greater absorber layer's thickness (W). Beyond a W= 1.0μm, JSC shows significant improvement, likely due to the enhanced absorption of longer wavelength photons within the thicker SWCNT layer. The fill factor (FF) in Fig. 3(c) exhibits a pattern similar to VOC, with significant variation after an acceptor concentration of 4×1017cm−3. At lower concentrations, FF is slightly higher, indicating that it does not follow a synchronized trend from the lowest to the highest values. The major output, efficiency (%η) in Fig. 3(d) peaks when the acceptor concentration is around 4×1019cm−3 and the thickness is approximately 1.5μm. At lower acceptor concentrations, FF shows a minor decrease with increasing SWCNT thickness, mainly due to the rise in the device's series resistance. Although achieving high doping levels across all materials is challenging, higher doping in SWCNT results in better efficiency. In summary, optimal performance for most parameters is achieved at a thickness of 1.5 μm. Except for JSC, the other three outputs reach their maximum values at an acceptor concentration of 1×1018cm−3. Although efficiencies above 32% can be obtained with an acceptor concentration as high as 1×1022cm−3, concentrations beyond 4×1019cm−3 are unsuitable due to the declining JSC.

Table. V

Ideal input parameters (thickness & acceptor concentration) and corresponding outputs under optimal conditions

Optimum Input Conditions		Outputs Parameters at Optimizing Input			
W(μm)	NA (cm−3)	VOC (V)	JSC (mA/cm2)	FF (%)	η (%)
1.5	4×1019	0.86	41.42	83.84	30.01

Table V provides a comprehensive summary of the optimal input conditions and the resulting output parameters for the proposed structure.

These output parameters demonstrate a significant improvement over those reported in previous SWCNT-based studies.

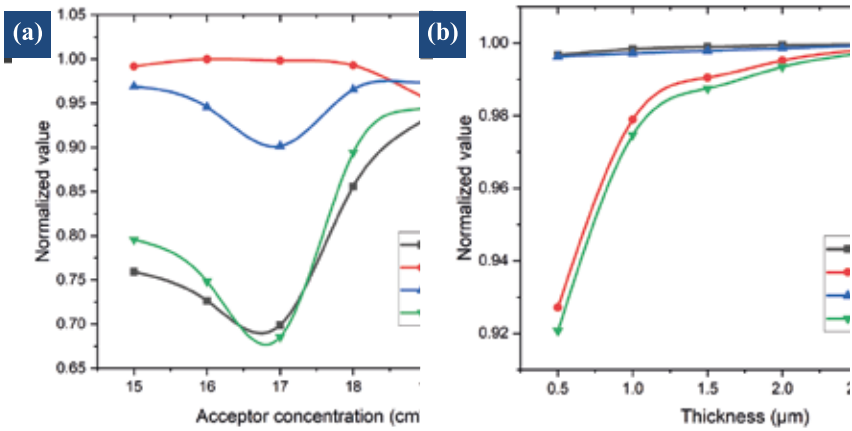

Figure. 4
Normalized plots of output parameters in relation to (a) Acceptor Concentration and (b) Absorber Layer Thickness.

Fig. 4 illustrates the normalized values of four outputs (VOC, JSC, FF, and efficiency (%η)), each plotted in relation to acceptor concentration in Fig. 4(a) and thickness in Fig. 4(b). These normalized values are calculated relative to the maximum values of their respective outputs. The optimum values were considered where highest efficiency (%η) is achieved while maintaining the other outputs (VOC, JSC, and FF) at relatively high levels. Under optimal input conditions (thickness W = 1.5μm and acceptor concentration NA = 4×1019cm-3, the normalized value of efficiency (%η) is near to the 1.0, and the other normalized outputs are 0.90 or higher.

3.3 Influence of defects density of the cell on PV performance

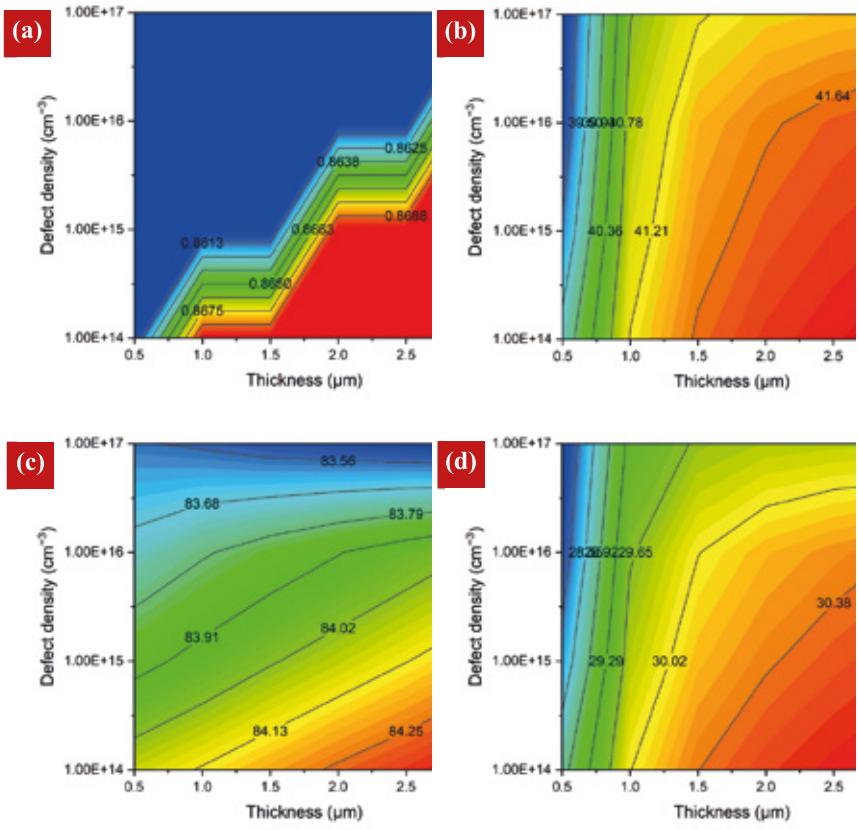

Figure. 5

Influence of defect density and absorber layer thickness on photovoltaic performance metrics ((a) VOC, (b) JSC, (c) FF, and (d) η (%)) of SWCNT-based solar cells.

To evaluate the device performance, Figure 5 illustrates the combined effects of absorber layer thickness and defect density on solar cell performance, with the acceptor concentration held constant at its optimal level. The analysis examines defect densities ranging from 1×1014cm−3 to 1×1017cm−3 and thicknesses from 0.5μm to 3.0μm. As shown in Fig. 5(a), the open circuit voltage (VOC) experiences minimal variation with changes in both thickness and defect density, ranging narrowly from 0.86V to 0.87V. This small variation indicates that VOC is relatively

stable, peaking at lower concentrations of both parameters and decreasing slightly but exponentially within this range. Figures 5(b) and 5(d) demonstrate that the short circuit current (JSC) and efficiency exhibit similar patterns in response to changes in thickness and defect density. Both JSC and efficiency are lower at higher defect densities and thinner absorber layers. Conversely, as defect density decreases and thickness increases, these outputs improve significantly, reaching higher values at low defect densities and greater thicknesses. Notably, both parameters achieve considerable performance at an absorber thickness of 1.5 μm. In Fig. 5(c), the fill factor (FF) follows a pattern akin to VOC, with only minor changes observed, fluctuating slightly from 83.45 mA/cm2 to 84.36 mA/cm2. This indicates that both VOC and FF are relatively unaffected by variations in defect density. Augmenting the thickness of the absorber layer has the potential to partially mitigate the negative impact of higher defect densities on performance. However, the presence of defects remains a limiting factor that cannot be entirely compensated by thickness alone.

3.4 Effects of series and shunt resistance

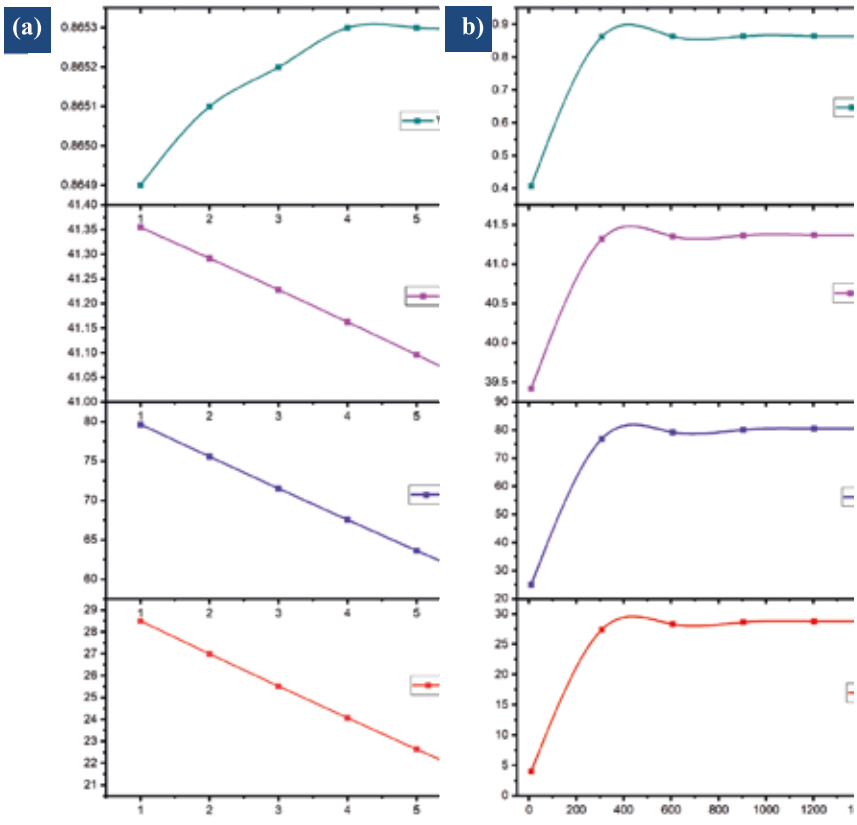

Figure. 6
Effect of series and shunt resistance on PV performace (VOC, JSC, FF, and PCE)

The efficiency of solar cells is significantly impacted by shunt resistance (RSh) and series resistance (RS), primarily arising from the connections between layers within the solar cell structure, metal contacts on either side, and defects from manufacturing (Hossain et al., 2022). Fig. 6(a) shows that Rs was varied from 0 to 6 Ω cm², whereas the shunt resistance was held constant at 105 Ω cm² for the Al/ITO/CdS/SWCNT/WS2/Pt structure. In Fig. 6(a), though it's showing ascending and descending curve in the output VOC and JSC, still the changes of this both outputs are very small, which can be ignored. In VOC, which varies the value from 0.8649V to 0.8653V and at JSC, the value varies from 41mA/cm2 to

41.30mA/cm2. In PSCs, series resistance (RS) arises from internal resistances, interface barriers, charge-collecting interlayers, and metal-based electrodes, while shunt resistance (RSh) is attributed to leakage pathways such as pinholes in the photoactive layer and recombination losses (Tvingstedt et al., 2017). Figure 6(b) illustrates the impact of varying RSh on VOC, JSC, FF, and PCE values, with RSh ranging from 0 to 1500 Ω cm². The performance parameters, including VOC, JSC, FF, and PCE, exhibit a similar trend as shunt resistance increases. All performance metrics increase rapidly from 0 Ω cm² to 600 Ω cm² and then stabilize as RSh continues to rise.

3.5 Effects of Temperature

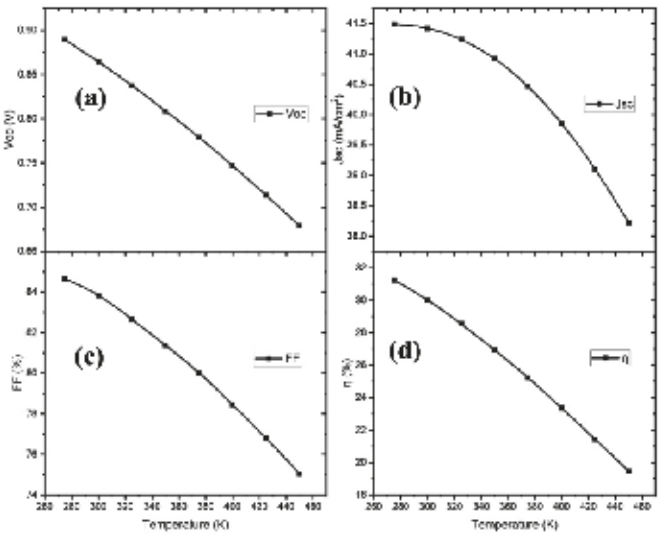

Figure. 7
Impact of temperature on performance metrics ((a) open circuit voltage (Voc), (b) short circuit current (Jsc), (c) fill factor (FF), and (d) efficiency (η%))

Understanding solar cell performance at elevated temperatures is vital for determining their stability. Many solar cell designs suffer from instability due to layer distortion at high temperatures. However, recent research in perovskite-based optoelectronics has shown improved stability and performance under these high-temperature conditions (Ma et al., 2020; Shi et al., 2018; Tvingstedt et al., 2017). To examine the impact of temperature on solar cell efficiency, the temperature range was varied from 275 K to 475 K. Fig. 7(a), Fig. 7(c), and Fig. 7(d) illustrate that as the temperature increases, the power conversion efficiency (PCE), fill factor

(FF), and open circuit voltage (VOC) decrease for nearly all optimal solar cell configurations. In Fig. 7(b) short circuit current has been decreasing slightly till the temperature 330 K then it's rapidly falling down with the increase of temperature.

3.6 QE Characteristics

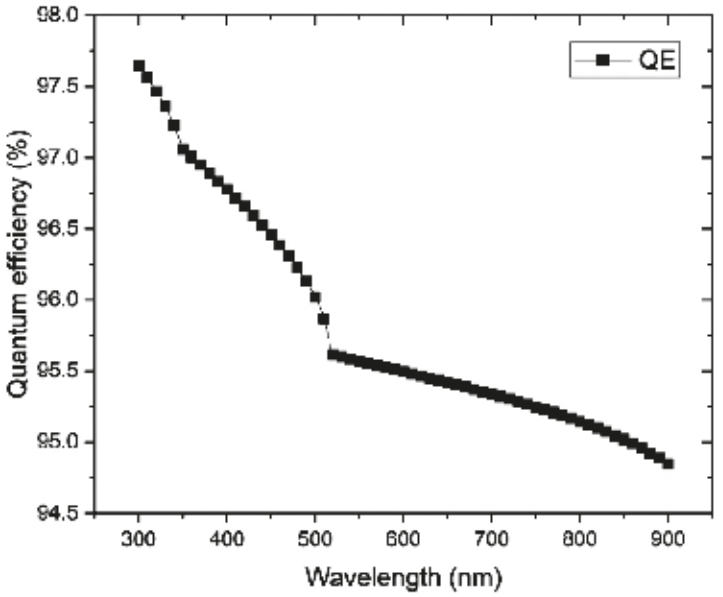

Figure. 8
QE curve of the proposed solar cell structure.

Figure 8 depicts the quantum efficiency (QE) curve across various wavelengths. The proposed configuration exhibited peak QE at 97.75% when the wavelength was 300 nm. And this structure showing its minimum value almost 95% at wavelength 900 nm. That means this structure showing the almost maximum QE at all over the wavelength. Nevertheless, recombination, where charge carriers are unable to enter an external circuit, reduces the quantum efficiency (QE) of most solar cells. The factors that influence collection probability also affect QE. For example, changes to the front surface can impact carriers generated near the surface. Moreover, highly doped front surface layers can lead to free carrier absorption, decreasing QE at longer wavelengths (Baker-Finch, McIntosh, Yan, Fong, & Kho, 2014).

3.7 Result comparison

Table. VI

Comparison of input conditions and obtained output parameters with previously published SWCNT-based work.

Structures	Optimum Input Parameters			Output Parameters				References
	Acceptor Concentration (cm^{-3})	Thickness (μm)	Defect Density (cm^{-3})	V_{OC} (V)	J_{SC} (mA/cm^2)	FF (%)	PCE (%)	
ITO/TiO_2/SWCNT/SnS	4×10^{21}	1.5	1×10^{14}	1.08	41.15	69.02	30.84	(Uddin, Rafi, Islam, Mominuzzaman, & Nath, 2022)
ITO/TiO_2/SWCNT/SnS	4×10^{21}	1.5	1×10^{16}	1.08	40.13	67.24	29.19	
ZnO/TiO_2/SWCNT/SnS	4×10^{20}	1.5	1×10^{15}	1.04	41.91	72.12	31.57	(Islam, Al Rafi, & Uddin, 2023)
ZnO/TiO_2/SWCNT/SnS	4×10^{20}	1.5	1×10^{16}	1.03	41.04	70.03	29.77	
ITO/CdS/SWCNT/WS_2	4×10^{19}	1.5	1×10^{16}	0.86	41.42	83.84	30.01	This work

Table VI shows the comparison of optimum input conditions and outputs of previous SWCNT-based solar cell structure with the newly proposed structure within this work. In this research, this work assessed the performance by modifying the absorber layer parameters and defect densities, while keeping other factors, including the electron transport material (ETM) and hole transport material (HTM) layers, consistent with those in prior simulation studies. The only exception was the donor concentration (N_D) of ITO, which was altered to enable thermionic emission. Also, another exceptional part of this work is visible in this table. The interesting part is that, as this work tried to keep higher defect density, so that higher defect densty also tried on the previous structures. And found those previously published published works, whose authors claim the higher efficiency that falls below 30%.

4. Conclusion

This research investigated and simulated the functionality of a hybrid heterojunction solar cell using a one-dimensional solar cell capacitance simulator (SCAPS-1D). The structure studied was ITO/CdS/SWCNT/WS_2. The outcomes of this study indicated that the lower thickness of the absorber layer substantially affects the device's core output- efficiency, with an optimal thickness identified at 1.5μm. The solar cell's efficiency improved with higher acceptor concentrations, reaching an optimal value at 4×10^{19} cm^{-3}. The model maintained a consistent defect density set at 1×10^{16} cm^{-3}. Additionally, it was observed

that increasing the operating temperature negatively impacts efficiency, with the best performance at 300°K. Under these optimal conditions, the solar cell achieved an efficiency of 30.01%, with an open circuit voltage of 0.86V, a short-circuit current of 41.42mA/cm^2, and a fill factor of 83.84%. The input parameters were chosen based on actual reported data from the literature, ensuring that the simulation outcomes were closely aligned with real-world conditions. This study demonstrates the significant potential of single-walled carbon nanotubes (SWCNTs) as absorber layers in heterostructure solar cells, providing a foundation for future studies on CNT-based solar cell configurations. The results underscore the importance of optimizing absorber layer properties to enhance the efficiency of solar cells using nanostructured materials.

References

Andreev, V. M. (1999). Heterostructure solar cells. *Semiconductors*, *33*(9), 942–945. https://doi.org/10.1134/1.1187808

Arnold, M. S., Blackburn, J. L., Crochet, J. J., Doorn, S. K., Duque, J. G., Mohite, A., & Telg, H. (2013). Recent developments in the photophysics of single-walled carbon nanotubes for their use as active and passive material elements in thin film photovoltaics. *Physical Chemistry Chemical Physics*, *15*(36), 14896–14918. https://doi.org/10.1039/C3CP52752B

Atowar Rahman, M. (2021). Enhancing the photovoltaic performance of Cd-free Cu2ZnSnS4 heterojunction solar cells using SnS HTL and TiO2 ETL. *Solar Energy*, *215*, 64–76. https://doi.org/10.1016/j.solener.2020.12.020

Bachilo, S. M., Strano, M. S., Kittrell, C., Hauge, R. H., Smalley, R. E., & Weisman, R. B. (2002). Structure-Assigned Optical Spectra of Single-Walled Carbon Nanotubes. *Science*, *298*(5602), 2361–2366. https://doi.org/10.1126/science.1078727

Baker-Finch, S. C., McIntosh, K. R., Yan, D., Fong, K. C., & Kho, T. C. (2014). Near-infrared free carrier absorption in heavily doped silicon. *Journal of Applied Physics*, *116*(6), 063106. https://doi.org/10.1063/1.4893176

Bati, A. S. R., Yu, L., Tawfik, S. A., Spencer, M. J. S., Shaw, P. E., Batmunkh, M., & Shapter, J. G. (2019). Electrically Sorted Single-Walled Carbon Nanotubes-Based Electron Transporting Layers for Perovskite Solar Cells. *iScience*, *14*, 100–112. https://doi.org/10.1016/j.isci.2019.03.015

Burgelman, M., Nollet, P., & Degrave, S. (2000). Modelling polycrystalline semiconductor solar cells. *Thin Solid Films*, *361–362*, 527–532. https://doi.org/10.1016/S0040-6090(99)00825-1

Dürkop, T., Getty, S. A., Cobas, E., & Fuhrer, M. S. (2004). Extraordinary Mobility in Semiconducting Carbon Nanotubes. *Nano Letters*, *4*(1), 35–39. https://doi.org/10.1021/nl034841q

Gorji, N. E., & Houshmand, M. (2013). Carbon nanotubes application as buffer layer in Cu(In,Ga)Se2 based thin film solar cells. *Physica E: Low-Dimensional Systems and Nanostructures*, *50*, 122–125. https://doi.org/10.1016/j.physe.2013.03.001

Hata, K., Futaba, D. N., Mizuno, K., Namai, T., Yumura, M., & Iijima, S. (2004). Water-Assisted Highly Efficient Synthesis of Impurity-Free Single-Walled Carbon Nanotubes. *Science*, *306*(5700), 1362–1364. https://doi.org/10.1126/science.1104962

Hossain, M. K., Rubel, M. H. K., Toki, G. F. I., Alam, I., Rahman, Md. F., & Bencherif, H. (2022). Effect of Various Electron and Hole Transport Layers on the Performance of CsPbI3-Based Perovskite Solar Cells: A Numerical Investigation in DFT, SCAPS-1D, and wxAMPS Frameworks. *ACS Omega*, *7*(47), 43210–43230. https://doi.org/10.1021/acsomega.2c05912

Idisi, D. O., & Mwakikunga, B. (2023). Two-dimensional layered metal dichalcogenides-based heterostructures for solar cells applications: A review. *Solar Energy*, *263*, 111981. https://doi.org/10.1016/j.solener.2023.111981

Islam, M. A., Al Rafi, J., & Uddin, M. A. (2023). Modeling and formation of a single-walled carbon nanotube (SWCNT) based heterostructure for efficient solar energy: Performance and defect analysis by numerical simulation. *AIP Advances*, *13*(11), 115201. https://doi.org/10.1063/5.0167228

Khatun, Most. M., Sunny, A., & Ahmed, S. R. A. (2021). Numerical investigation on performance improvement of WS2 thin-film solar cell with copper iodide as hole transport layer. *Solar Energy*, *224*, 956–965. https://doi.org/10.1016/j.solener.2021.06.062

Ma, Z., Shi, Z., Qin, C., Cui, M., Yang, D., Wang, X., … Shan, C. (2020). Stable Yellow Light-Emitting Devices Based on Ternary Copper Halides with Broadband Emissive Self-Trapped Excitons. *ACS Nano*, *14*(4), 4475–4486. https://doi.org/10.1021/acsnano.9b10148

Nazif, K. N., Kumar, A., Menezes, M. T. M. de, & Saraswat, K. (2019). Towards high Voc, thin film, homojunction WS2 solar cells for energy harvesting applications. *Wide Bandgap Materials, Devices, and Applications IV*, *11126*, 1112606. SPIE. https://doi.org/10.1117/12.2533007

Niu, T., Xie, Y.-M., Xue, Q., Xun, S., Yao, Q., Zhen, F., … Cao, Y. (2022). Spacer Engineering of Diammonium-Based 2D Perovskites

toward Efficient and Stable 2D/3D Heterostructure Perovskite Solar Cells. *Advanced Energy Materials*, *12*(2), 2102973. https://doi.org/10.1002/aenm.202102973

Oublal, E., Ait Abdelkadir, A., & Sahal, M. (2022). High performance of a new solar cell based on carbon nanotubes with CBTS compound as BSF using SCAPS-1D software. *Journal of Nanoparticle Research*, *24*(10), 202. https://doi.org/10.1007/s11051-022-05580-7

Parida, B., Iniyan, S., & Goic, R. (2011). A review of solar photovoltaic technologies. *Renewable and Sustainable Energy Reviews*, *15*(3), 1625–1636. https://doi.org/10.1016/j.rser.2010.11.032

Rahman, M. A. (2021). Design and simulation of a high-performance Cd-free Cu2SnSe3 solar cells with SnS electron-blocking hole transport layer and TiO2 electron transport layer by SCAPS-1D. *SN Applied Sciences*, *3*(2), 253. https://doi.org/10.1007/s42452-021-04267-3

Ray, M., & Chakraborty, B. (2021). Impact of demand response on escalating energy access with affordable solar photovoltaic generation in the Global South. *Renewable and Sustainable Energy Reviews*, *143*, 110884. https://doi.org/10.1016/j.rser.2021.110884

Scheer, H. (2004). *The Solar Economy: Renewable Energy for a Sustainable Global Future*. London: Routledge. https://doi.org/10.4324/9781849773928

Schöppler, F., Mann, C., Hain, T. C., Neubauer, F. M., Privitera, G., Bonaccorso, F., … Hertel, T. (2011). Molar Extinction Coefficient of Single-Wall Carbon Nanotubes. *The Journal of Physical Chemistry C*, *115*(30), 14682–14686. https://doi.org/10.1021/jp205289h

Schroder, D. K., & Meier, D. L. (1984). Solar cell contact resistance—A review. *IEEE Transactions on Electron Devices*, *31*(5), 637–647. https://doi.org/10.1109/T-ED.1984.21583

Shi, Z., Li, S., Li, Y., Ji, H., Li, X., Wu, D., … Du, G. (2018). Strategy of Solution-Processed All-Inorganic Heterostructure for Humidity/Temperature-Stable Perovskite Quantum Dot Light-Emitting Diodes. *ACS Nano*, *12*(2), 1462–1472. https://doi.org/10.1021/acsnano.7b07856

Subash, S., & Chowdhury, M. H. (2009). High efficiency carbon nanotube based solar cells for electronics devices. *Proceedings of the 2009 12th International Symposium on Integrated Circuits*, 240–243. Retrieved from https://ieeexplore.ieee.org/abstract/document/5403959

Tune, Daniel D., Hennrich, F., Dehm, S., Klein, M. F. G., Glaser, K., Colsmann, A., … Flavel, B. S. (2013). The Role of Nanotubes in Carbon Nanotube–Silicon Solar Cells. *Advanced Energy Materials*, *3*(8), 1091–1097. https://doi.org/10.1002/aenm.201200949

Tune, Daniel David, & Shapter, J. G. (2013). The potential sunlight harvesting efficiency of carbon nanotube solar cells. *Energy & Environmental Science*, *6*(9), 2572–2577. https://doi.org/10.1039/C3EE41731J

Tvingstedt, K., Gil-Escrig, L., Momblona, C., Rieder, P., Kiermasch, D., Sessolo, M., … Dyakonov, V. (2017). Removing Leakage and Surface Recombination in Planar Perovskite Solar Cells. *ACS Energy Letters*, *2*(2), 424–430. https://doi.org/10.1021/acsenergylett.6b00719

Uddin, M. A., Rafi, J. A., Islam, Md. A., Mominuzzaman, S. M., & Nath, I. D. (2022). Modeling and Numerical Analysis of Heterostructure Single-Walled Carbon Nanotube (SWCNT) Solar Cell. *2022 12th International Conference on Electrical and Computer Engineering (ICECE)*, 388–391. https://doi.org/10.1109/ICECE57408.2022.10089020

Wang, L., Liu, H., Konik, R. M., Misewich, J. A., & Wong, S. S. (2013). Carbon nanotube-based heterostructures for solar energy applications. *Chemical Society Reviews*, *42*(20), 8134–8156. https://doi.org/10.1039/C3CS60088B

Xosrovashvili, G., & Gorji, N. E. (2014). Numerical Simulation of Carbon Nanotubes/GaAs Hybrid PV Devices with AMPS-1D. *International Journal of Photoenergy*, *2014*, e784857. https://doi.org/10.1155/2014/784857